JOURNAL OF THERMOPHYSICS AND HEAT TRANSFER
Vol. 8, No. 1, Jan.–March 1994

Experimental Investigation of a Nitrogen High-Enthalpy Flow

Stefanos Fasoulas,* Monika Auweter-Kurtz,† and Harald A. Habiger‡
Institut für Raumfahrtsysteme, Universität Stuttgart, D-70550 Stuttgart 80, Germany

This article presents experimental results of a nitrogen high-enthalpy plasma flow obtained within a test campaign at the Institut für Raumfahrtsysteme. Different measurement techniques have been applied to determine the flowfield properties in flow direction and the distributions at two cross sections, i.e., pressure, heat flux, velocity, electron density, and temperature measurements. These measurements make possible the calculations of the local specific enthalpy and the mass flux distributions of the plasma plume. The experimental data at the first cross section are to be used as initial and boundary conditions, the comparison of the calculated and experimental results at the second cross section allow the verification of the models used in numerical codes.

I. Introduction

TWO plasma wind tunnels (PWK[1–3]) were built-up at the Institut für Raumfahrtsysteme (IRS) of the University of Stuttgart for the simulation of re-entry or entry conditions with high specific enthalpies and low pressures as required, e.g., for the development of modern oxidation protected materials for the thermal protection system (TPS) of HERMES (Fig. 1). The wind tunnels are connected to a power supply of 6 MW and a roots pump system with a total suction power of more than 250,000 m³/h. They are equipped with a magnetoplasmadynamic (MPD) plasma source[4] (Fig. 2) designed for a power level up to 0.5 MW, and for specific enthalpies ranging from 5 MJ/kg up to more than 150 MJ/kg in order to simulate the first phase of the re-entry where the specific enthalpy is high and the temperature is at its maximum. The stagnation pressure reaches from 0.1 mbar up to 50 mbar; the maximum mass flow with air is at the moment about 30 g/s.

The continuously operating plasma wind tunnels are the only tool readily available to investigate the surface chemistry associated with the erosion behavior of candidate TPS materials. In these facilities the emphasis is placed on reproducing thermophysical and chemical similarities on the surface of the tested specimen rather than aerodynamic similarities. While the PWK1 is mainly used for the experimental investigation of materials, the PWK2 partly serves the development of diagnostic methods for the characterization of plasma wind-tunnel conditions and erosion or ablation mechanisms. Furthermore, PWK2 is used for the simulation of the entry conditions into atmospheres of other celestial bodies like Titan and Mars.

Several experimental methods are available or under development for plasma plume investigation: the Pitot probe; stationary and transient heat flux probe; enthalpy probe measurements in the plasma plume; electrostatic probes to measure the plasma potential, heavy particles velocity, electron temperature and density; catalytic thermocouple probes to detect the atomic oxygen flux. Monitoring of the specimen front and rear side temperature by pyrometers is also in use,[5] and a Fabry-Perot interferometer has been put in operation to measure the plasma velocity and heavy particles kinetic temperature. Emission spectroscopic investigation of the plume is being qualified for plasma thrusters and is planned to be applied to examine the PWK. A mass spectrometer including an energy analyzer for the investigation of the plasma state in front of the specimen is also being qualified at present.

All mechanical and electrostatic probes are mounted on a platform with four motor driven axes. Three of these axes are linearly oriented. The fourth one provides the possibility to rotate the probes. The moving range of the platform is 750

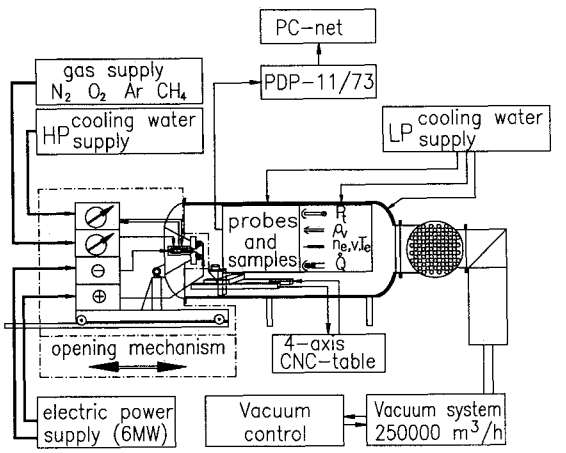

Fig. 1 Scheme of PWK-IRS.

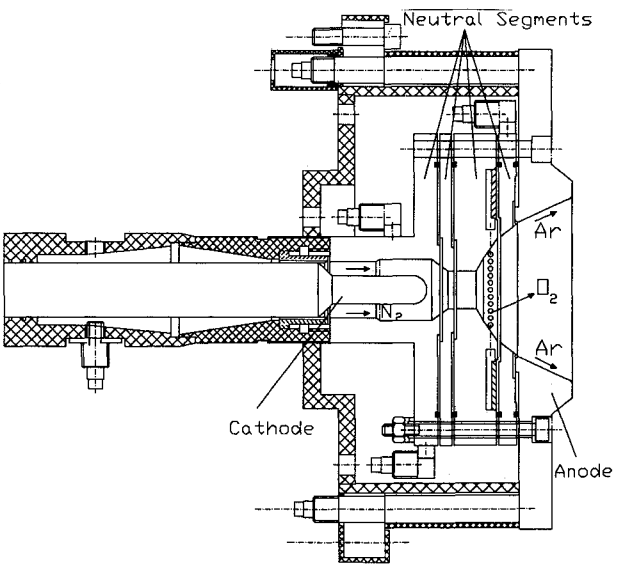

Fig. 2 Scheme of the plasma source MPD-RD2.

Received Nov. 16, 1992; revision received March 8, 1993; accepted for publication March 23, 1993.

*Research Engineer, Electric Propulsion and Plasma Technology Division.

†Professor, Head Electric Propulsion and Plasma Technology Division. Member AIAA.

‡Research Scientist, Electric Propulsion and Plasma Technology Division. Member AIAA.

mm in x direction, which is defined as the distance to the plasma source, and 400 mm in y direction, symmetric to the jet axis centerline. The possible vertical lift is about ±75 mm to the centerline. The maximum velocity in the xy plane is about 5 cm/s.

The experimental part of the PWK facility investigations is accompanied by computations of the flowfield properties. This is especially important for the understanding of the prevailing complex physicochemical phenomena, including chemical and thermal nonequilibrium in the plasma wind tunnels. Furthermore, since complete measurements of all parameters in the complex plasma wind-tunnel environment are not possible, some parameters have to be determined by using numerical methods. It is apparent that these codes have to be validated by experimental determination of the accessible parameters. For this reason an experimental survey was performed to get the necessary data.[6,7]. Most of the measurement techniques mentioned above were applied for the determination of the flowfield properties at two cross sections of a pure nitrogen plasma flow. The measurement results at the first section should serve as initial and boundary conditions (inflow cross section). The results at the second section (outflow cross section) should give the possibility to compare them with the calculated values of the numerical codes.

II. Test Conditions

The nitrogen plasma flow examined within this experimental program should simulate the conditions which result in a maximum calculated temperature at the leading edge for the re-entry of HERMES.[8] The parameters for the flight environment are; altitude Z = 81.3 km, a velocity v = 7452 m/s which corresponds to a specific freestream enthalpy h_∞ = 28 MJ/kg, a specific mass flow rate $\dot{m}_1$ = 0.117 kg/(m²s), and a total pressure of p_{tot} = 4 mbar.

Because these conditions are not directly adjustable within the plasma wind tunnel, an interpolation procedure was necessary to obtain the necessary values for the current, mass flux, ambient pressure, and the distance to the plasma source. For the interpolation, in a first step, the total mass flux which is necessary to achieve the local specific mass flux rate was calculated from a global pressure distribution function. In a second step, the necessary position to reach the total pressure was determined. Therefore, the mass flux was kept constant, whereas the ambient pressure, the distance from the anode, and the current were varied. As a third and last iteration step, the heat flux at the specified test points was measured in order to obtain a first approximation of the local specific enthalpy of the jet with the theory of heat transfer.

The directly adjustable parameters which were obtained after this procedure are; total mass flux of 1.33 g/s nitrogen, current of 750 A, ambient pressure of 2.9 mbar, and distance of 300 mm to the plasma source. The total power input is about 38 kW at these conditions. The position x = 300 mm was chosen simultaneously as the outflow cross section of the program. The inflow cross section was fixed at a position of 50 mm.

III. Pitot Pressure Measurements

With pitot tubes it is possible to measure the dynamic or stagnation pressure of the plasma jet through connection to either a differential or a total pressure gauge, respectively inside or outside of the vacuum tank. Measuring the dynamic pressure with a differential pressure gauge, the stagnation pressure is determined as the sum of dynamic and ambient pressure. The ambient pressure is measured outside of the jet and can be adjusted by regulating the vacuum system. The pitot probe used during this test program is a new development with identical geometry as the material support system used for material tests (Fig. 3). In Fig. 4 the total pressure vs the axial position obtained with the pitot probe is depicted.

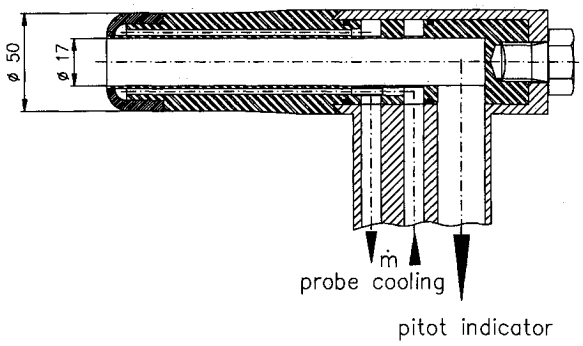

Fig. 3 Pitot probe.

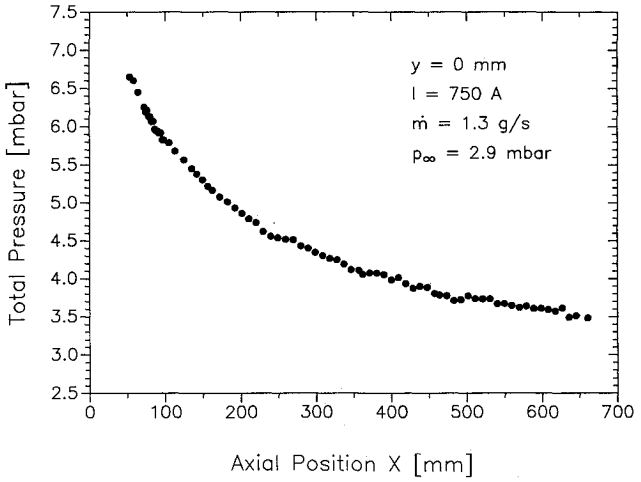

Fig. 4 Total pressure vs axial position.

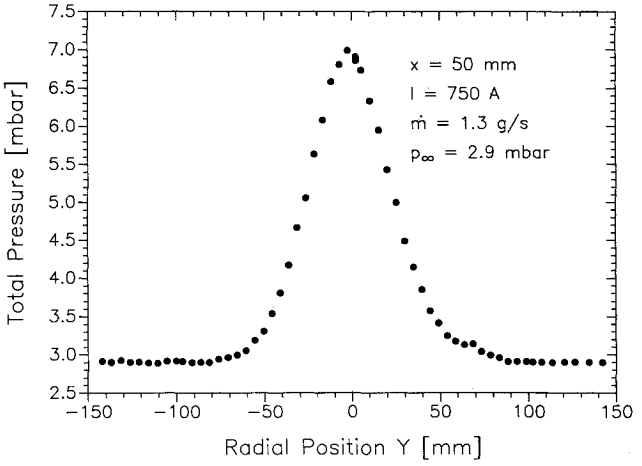

Fig. 5 Total pressure vs radial position at a distance of x = 50 mm.

The radial distributions of the pressure at the two specified cross sections are shown in Figs. 5 and 6.

The accuracy of the total pressure measurements may be estimated to be within 5%. The possible error sources and their influences are 1) fluctuations of the vacuum system (±2%); 2) fluctuations of the plasma jet with increasing distance x to the anode (max ±2%); 3) accuracy of the differential pressure gauge (±0.5%); 4) deviations in reproducing and adjusting the test conditions (max ±0.3%); and 5) rarefied gas effects (negligible).

IV. Heat Flux Measurements

The description of aerodynamic heat transfer within a plasma flow is complicated by features which are not present in nor-

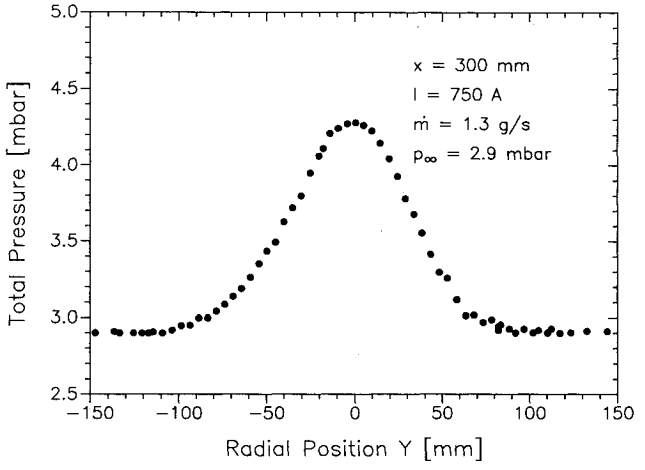

Fig. 6 Total pressure vs radial position at a distance of x = 300 mm.

mal gas flows. A first feature is the possible dissociation and/or ionization of the gas due to the high temperatures encountered where the gas is decelerated by shock waves and viscous forces in the boundary layer or at a stagnation point. Because dissociation and ionization and their reverse processes (recombination) proceed at finite rates, thermochemical equilibrium is not necessarily achieved throughout the flowfield. Furthermore, diffusion of atoms and ions to the wall, which subsequently recombine by setting free their specific recombination energy, should be taken into account in addition to the heat transferred by normal conduction. Radiative transport may also occur, but is very difficult to calculate. Taking all these features into consideration, it is obvious that the heat transfer to a body exposed to a plasma flow, as within the PWK, may vary depending on the material of the body (total, partial, or noncatalytic surface), its surface temperature which affects the recombination rate and its emission coefficient.

Heat flux measurements are normally performed using copper bodies. The stationary and transient heat flux measurements with such copper probes may therefore be treated only as an estimation of the actual existing heat flux during a real material test. The heat flux is measured at IRS by calorimeters which are geometrically very similar to the material support system used within the HERMES program. The actual probes are inserts into the front plate of a water-cooled device and consist of either a heat sink copper slug for transient heat flux measurements or a water-cooled tube for stationary measurements. These inserts are insulated thermally from the surrounding support. When the probe is moved into the plasma jet only the heat flux to the front side facing the plasma is measured. The cylindrical surface is shielded with a separately water-cooled jacket. The area of the insert which is exposed to the plasma is similar to the area of typical samples within the HERMES program. The stationary heat flux probe is shown in Fig. 7. The transient probe has nearly the same shape, only the probe cooling water circuit is not used and the copper insert is equipped with two thermocouples.

For the stationary case, the flow rate $\dot{m}_W$ and the temperature difference of the incoming and outgoing water ($T_{W,\text{out}} - T_{W,\text{in}}$) are measured, the latter by thermocouples which are coated in order to avoid an influence by the plasma potential. The heat flux per unit area is then given by

$$\dot{q} = [c_W \dot{m}_W (T_{w,\text{out}} - T_{W,\text{in}})/A] \tag{1}$$

where c_W is the heat capacity of water, and A the surface area of the probe.

For the transient heat flux determination, the temperature increase in the copper slug is measured with two thermocouples at different positions. The first thermocouple is placed

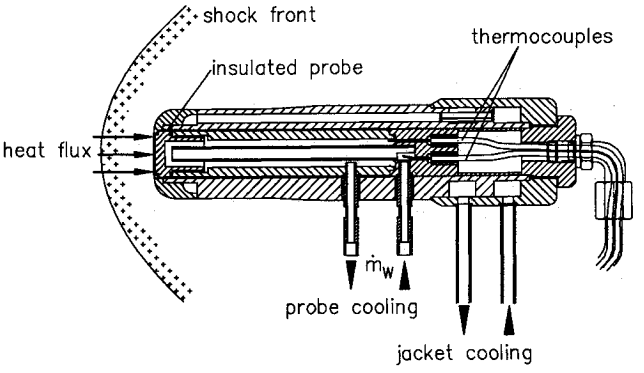

Fig. 7 Stationary heat flux probe.

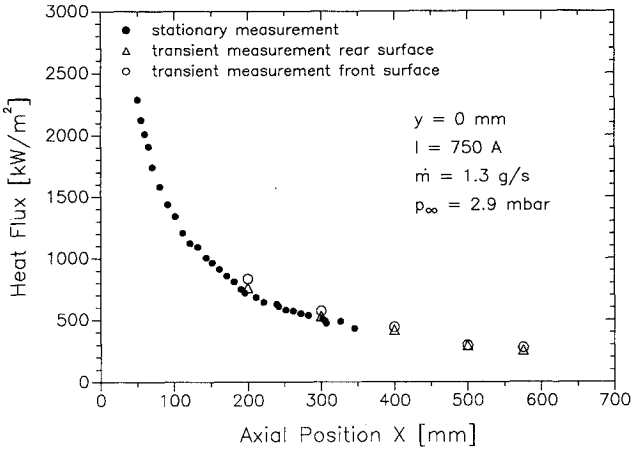

Fig. 8 Heat flux vs axial position.

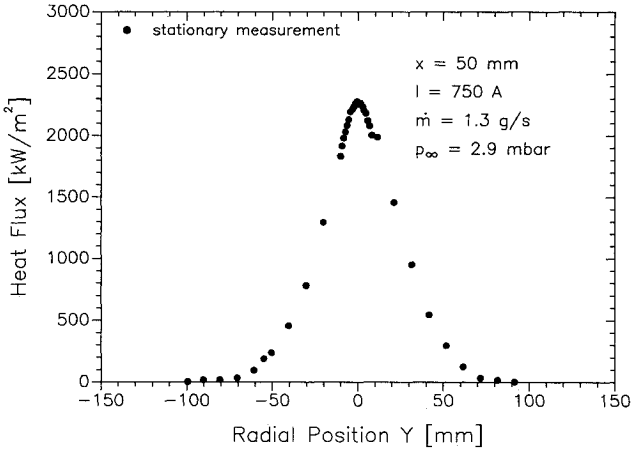

Fig. 9 Heat flux vs radial position at a distance of x = 50 mm.

through a bore-hole at a distance x = 0.1 mm from the front surface, the second one at the back surface of the slug. The heat flux may then be determined as[9]

$$\dot{q} = \rho c_p s \frac{\mathrm{d}T}{\mathrm{d}t} \tag{2}$$

where c_p is the heat capacity of copper, ρ the density of copper, s the probe thickness, and $\mathrm{d}T/\mathrm{d}t$ the temperature increase with respect to time.

The results of the stationary and transient heat flux measurements as axial and radial profiles at the specified test conditions are shown in Figs. 8–10. As expected, the heat flux increases rapidly with decreasing distance to the plasma

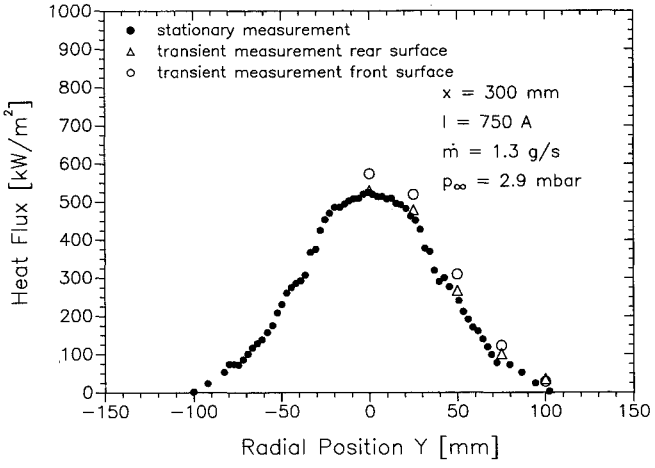

Fig. 10 Heat flux vs radial position at a distance of x = 300 mm.

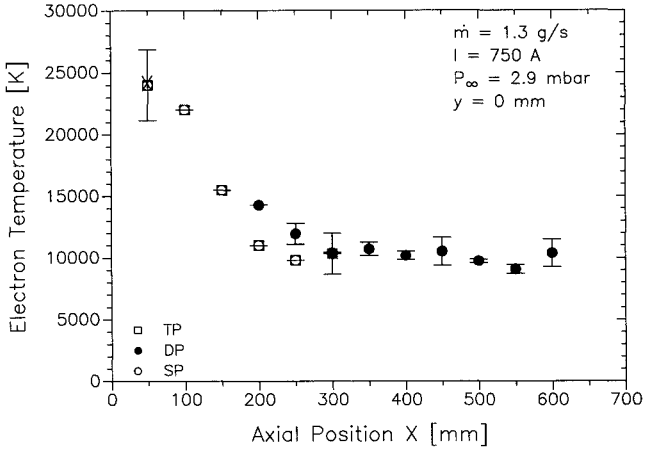

Fig. 11 Axial electron temperature distribution.

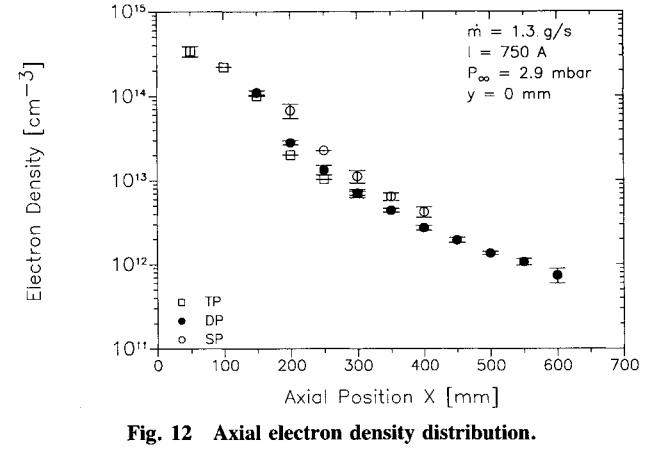

Fig. 12 Axial electron density distribution.

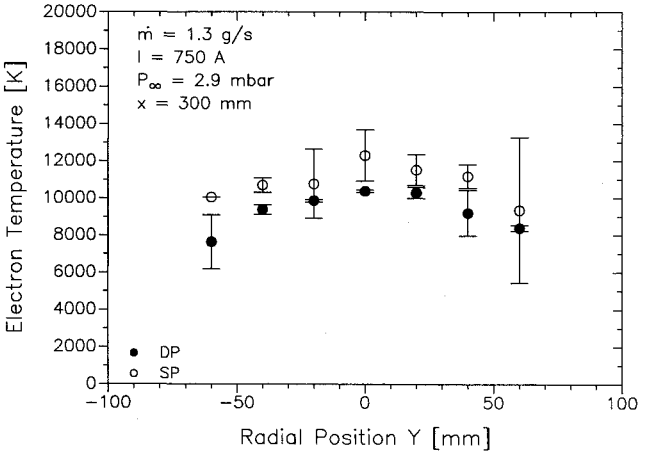

Fig. 13 Radial electron temperature distribution at x = 300 mm.

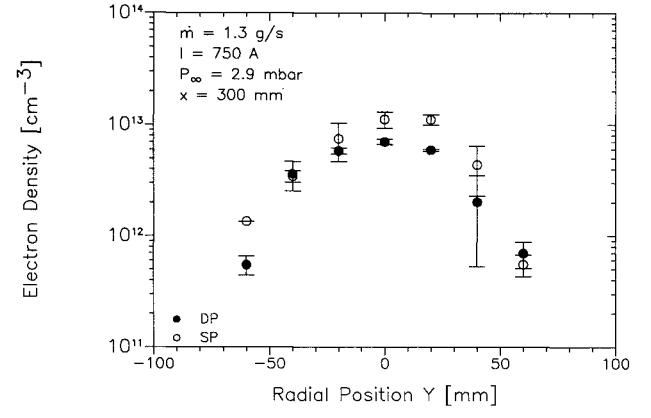

Fig. 14 Radial electron density distribution at x = 300 mm.

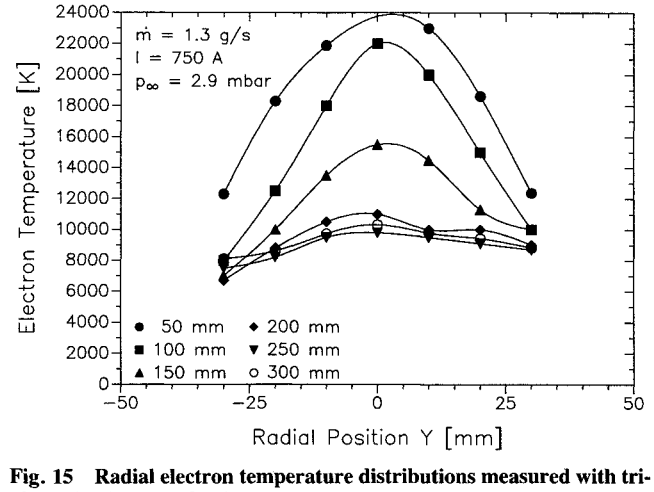

Fig. 15 Radial electron temperature distributions measured with triple probe (mean values).

source and shows a smooth drop with increasing distance downstream in the tunnel. The radial heat flux profiles are very similar to the pressure profiles.

Besides the effects mentioned in the description of the pitot pressure measurements, the stationary and transient heat flux determination is additionally affected by the accuracy of the thermocouple temperature difference measurement, the water flow meter, and the effective diameter of the copper slug.

V. Electrostatic Probe Measurements

For the present research program, electrostatic probes[3,10] were used to determine the electron temperature T_e and electron number density n_e at different axial and radial positions in the freestream plasma jet. Different types of probes were used to check the reliability of single measurements.

An electrostatic (Langmuir) probe consists of a metallic electrode placed inside a plasma.[11] The measurement method is applied to obtain a voltage-current characteristic for single and double probes. For single probes, the vacuum chamber is used as reference electrode, whereas for double probes two electrodes of equal or different areas are used. The two electrodes have to be separated by a certain distance d so that they do not disturb each other ($d > \lambda_d$, the Debye length).

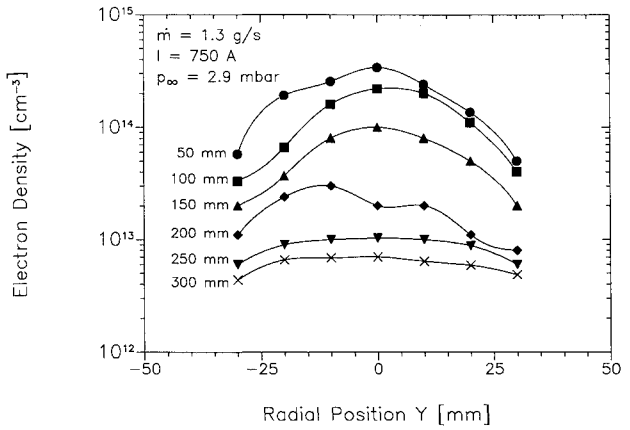

Fig. 16 Radial electron density distributions measured with triple probe (mean values).

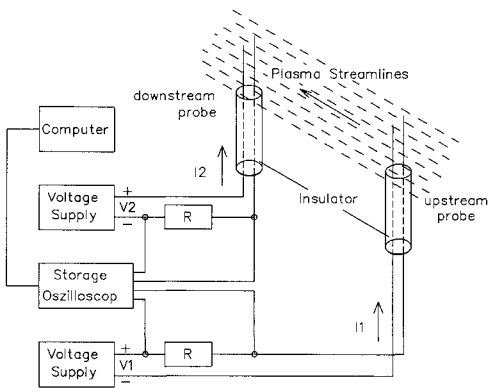

Fig. 17 Time of flight probe experimental setup.

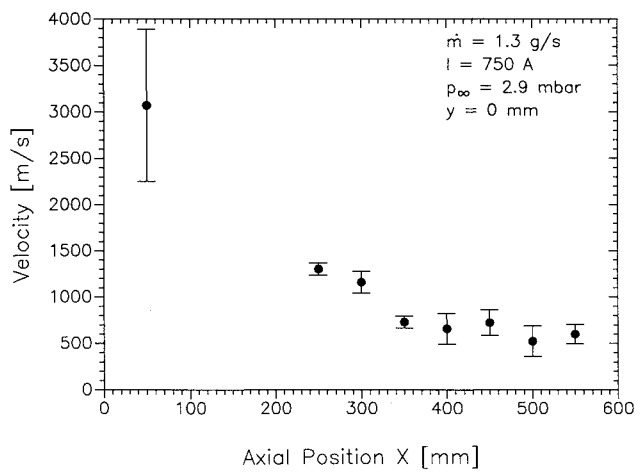

Fig. 18 Axial plasma velocity distribution.

An electrostatic probe system which allows an immediate direct display of the electron temperature and electron number density, without intensive characteristic evaluation, is the triple probe.[12] It consists of three symmetrical electrodes of surface area A, two of them connected as a double probe and a third floating with respect to the plasma.

For the determination of electron temperatures and electron number densities, several measurements per test point with single, double, and triple probes (SP, DP, TP) were performed.[6,7] The measurements were taken at different axial positions with the single and double probes. With both kinds of probes and with the triple probe, a radial scan at an axial distance of 300 mm was also performed. The results presented

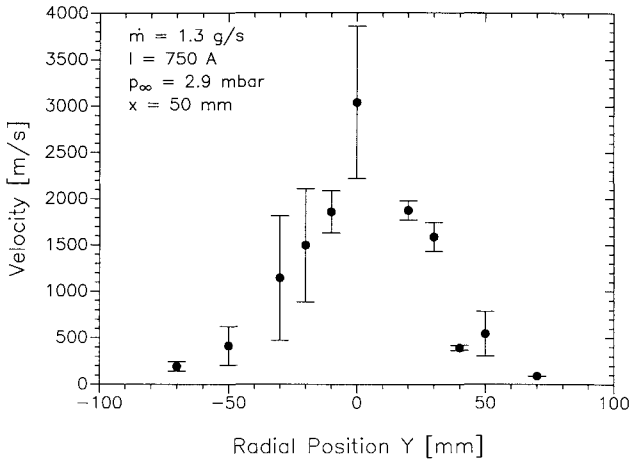

Fig. 19 Radial plasma velocity distribution at an axial distance of x = 50 mm.

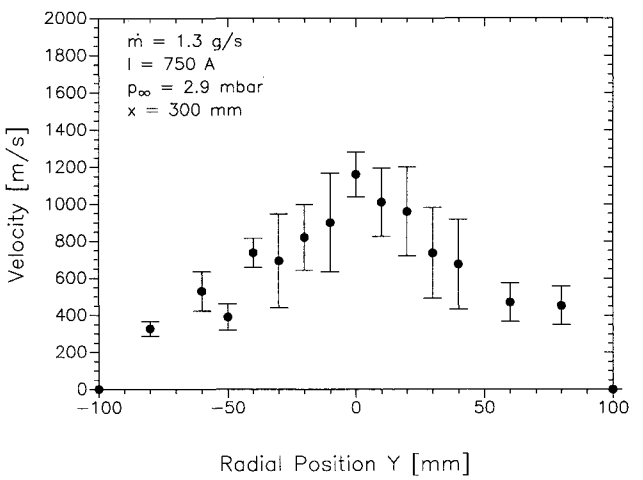

Fig. 20 Radial plasma velocity distribution at an axial distance of x = 300 mm.

below for single and double probes are mean values, the error bars are standard deviations. In Figs. 11 and 12 the axial distributions of the electron temperature and the electron density in the centerline of the plasma jet are shown. The results show good agreement between the two types of probes and the applied evaluation theories.

In Figs. 13 and 14, comparisons of radial measurements with single and double probes are shown. The electron temperature at the plasma centerline at an axial distance of 300 mm was determined to be about 10,500 K, the electron density is about 10^{13} 1/cm³.

A radial profile of the nitrogen plasma jet at an axial distance of x = 50 mm was the subject of further investigations with the triple probe. For the determination of the electron temperature and electron number density, several measurements were taken by a radial motion through the plasma jet. The results shown in Figs. 15 and 16 are radial profiles of mean values which were obtained by averaging the values of several measurements.

The electron temperature in the plasma centerline at an axial distance of x = 50 mm was determined to be about 24,000 K. The electron density increases from close to 10^{13} 1/cm³ at 300 mm to 10^{14} 1/cm³ at 50 mm.

The next application of electrostatic probes is the measurement of the plasma velocity by time of flight (TOF) probes. The experimental setup is shown in Fig. 17. Time of flight probes[13] are electrostatic probes separated at a known distance and aligned with the flow of the plasma particles. Dou-

ble probes are most convenient for TOF probes because they are not affected by fluctuations of the plasma potential between widely separated electrodes while floating with the plasma potential, like in the single probe case. Upstream and downstream probes are both biased to draw ion-saturation current. Fluctuations in the local ion number density around a probe result in fluctuations in the detected ion current. By moving with the flow velocity, those fluctuations are first detected at the upstream probe and then time delayed at the downstream probe. The method of the time of flight probes as described is only applicable within freestream conditions. The time shift of both signals can clearly be determined by performing a fast Fourier transform (FFT) cross-correlation with the two signals, the exact value of the time shift and the time of flight are easily determinable. By the known separation of the two probes, the velocity of the heavy particles can be calculated.

Figure 18 shows the axial velocity distribution at the center of the plasma jet. In order to obtain a good time resolution, the distance of the two double probes was set to 52 mm, the center between the probes was located at the axial test position. So far, the average value of the velocity gradient between the two probe positions was detected as the plasma velocity. The values of the velocity are mean values out of four measurements at each position, errors are given as standard deviations of the mean values.

Because the detected plasma velocities are lower than expected, it seems reasonable to decrease the probe separation in order to decrease the time of flight. This means a smaller time constant for the diffusion of the ion density fluctuations, which results in a better cross correlation of the upstream and downstream signals. For the measurements at $x = 50$ mm, the radial velocity profile was taken with a probe separation of 25 mm. For comparison, a radial profile at $x = 300$ mm was taken with the new probe separation. The profiles are shown in Figs. 19 and 20.

The centerline velocity at the axial distance of 50 mm is about 3000 m/s, and at 300 mm about 1000 m/s. The velocity measurements, especially those close to the plasma source, are to be verified by optical velocity measurements using the Doppler effect detected with a Fabry-Perot interferometer.

VI. Specific Enthalpy

The specific enthalpy is an important parameter for the heat load simulation of TPS materials. Therefore, a precise analysis of the experimental conditions as well as the numerical evaluation is crucial.

In order to carry out first estimations of the specific enthalpy of the plasma jet in the PWK, the average specific enthalpy at the end of the plasma source is determined. For this purpose the flow rate of the cooling water of the plasma source is measured. Combined with a temperature difference measurement between incoming and outgoing water, all heat losses inside the plasma source can be evaluated. Since the power input is also known, given by the product of current and voltage, the enthalpy of the plasma jet at the nozzle exit is easily obtained as the difference between the electric power input and the total heat loss within the plasma accelerator. This calculated enthalpy related to the gas flow gives the average total specific enthalpy at the end of the plasma source nozzle. For the present test program this average enthalpy of the plasma jet is about 19.3 MJ/kg. It is obvious that this mean enthalpy results from a local distribution of the specific enthalpy.

A method to investigate the local specific enthalpy in the freestream plasma flow is given by the theory of heat transfer. Two methods to determine the local specific enthalpy will be presented in the following.

A. First Method

The authors in Refs. 14–16 approximated a relationship between the heating rate and the enthalpy for a frozen freestream flow as

$$\dot{q}_{fc} = K(p_{tot}/R_{eff})^{0.5} h_{t,e} \tag{3}$$

where K is assumed to be a constant, $h_{t,e}$ being the total specific enthalpy at the boundary-layer edge which may be assumed to be equal to the freestream enthalpy $h_{t,\infty}$, $\dot{q}_{fc}$ being the equivalent fully catalytic heat flux, and R_{eff} an effective probe nose radius given by[17,18] $R_{eff} = 2.9\ R_f$ for a flat-faced probe with radius R_f. Although the temperature of the copper surface of the heat flux probes is relatively low, it may not be considered fully catalytic with respect to the recombination of the atoms. Goulard[19] and Pope[17] derived a theory which allows the calculation of the ratio of the heating rate at a partially catalytic surface to the equivalent heating rate at a fully catalytic surface. This ratio depends on the local freestream enthalpy. This method was used here to calculate the equivalent fully catalytic heat flux from the measured heat flux on the copper probe.

With the known pressure distribution at these positions (Figs. 5 and 6) it is now possible to calculate the local specific enthalpy distributions (Fig. 21), and in addition to determine a mean specific enthalpy by integrating the local enthalpy distribution. The calculated mean values are also depicted in Fig. 21. The average enthalpy of 21.5 MJ/kg at the inflow cross section ($x = 50$ mm) compares well with the mean enthalpy determined at the plasma source exit (19.3 MJ/kg). On the other hand, the mean value at the outflow cross section ($x = 300$ mm) of 7.6 MJ/kg indicates losses of specific energy of the plasma flow, which may be caused by radiation or by sucking in and accelerating the ambient gas. The latter would increase the total mass flow of the jet, and therefore decrease the specific energy. The maximum specific enthalpy calculated with Eq. (3) is 85.9 MJ/kg at $x = 50$ mm and 26.6 MJ/kg at $x = 300$ mm, respectively, at the center of the jet.

Small losses of the specific energy were estimated to be due to radiation (about 5%).[20,21] Therefore, the ratio of the energy losses by suction of ambient gas will be about 2.4. The total mass flux rate at the position $x = 300$ mm should then be about 3.2 g/s.

B. Second Method

The relationship used in the theory derived by Fay and Riddell[22] to determine the local specific enthalpy is more detailed. They suggested a correlation equation which best rep-

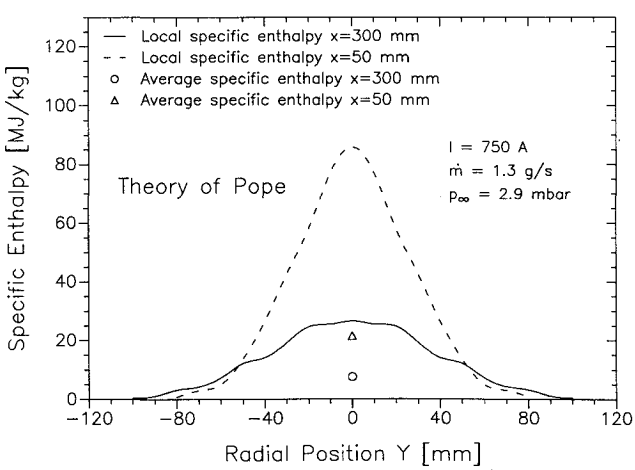

Fig. 21 Local specific enthalpy distribution according to Refs. 14–16.

resented their numerical integration of the heat flux on a fully catalytic wall (see also Ref. 23)

$$\dot{q}_{fc} = 0.937(\rho_s\mu_s/\rho_\infty\mu_\infty)^{0.1}(\beta\rho_\infty\mu_\infty)^{0.5}(h_{t,\infty} - h_s) \qquad (4)$$

where ρ and μ are the density and the absolute viscosity, and the subscripts s and ∞ denote stagnation point and freestream values, respectively. The values for the absolute viscosity may be determined for a given temperature according to the theories outlined in Ref. 6. Based on temperature measurements at the center of the jet, the radial temperature distributions

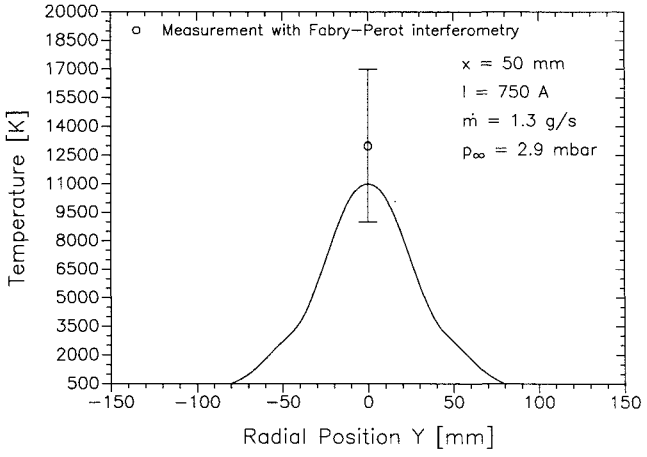

Fig. 22 Temperature distribution at a distance of x = 50 mm.

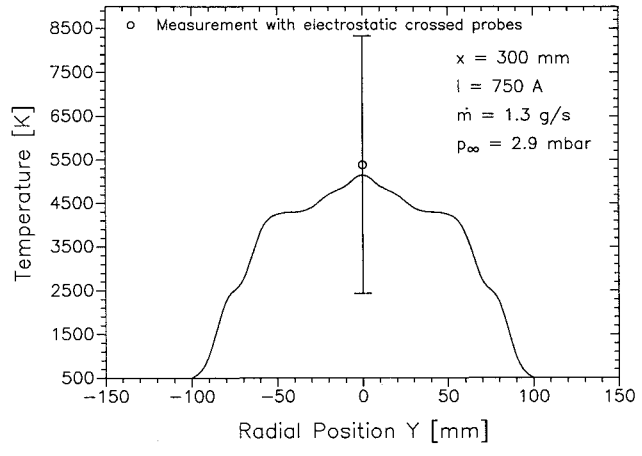

Fig. 23 Temperature distribution at a distance of x = 300 mm.

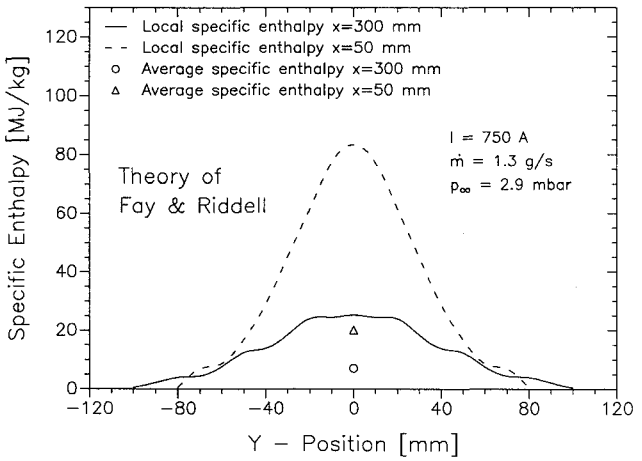

Fig. 24 Local specific enthalpy distribution according to Refs. 22 and 23.

were estimated as shown in Figs. 22 and 23. Therefore, the ratio of the electron temperature to the heavy particle temperature was about 2.0 for the position x = 300 mm and 2.2 for x = 50 mm.

Because of the chemical and thermodynamic nonequilibrium of the flow, the values for the molecular mass M_M for the gas mixture and the ratio of the specific heats κ are not known exactly. They can be calculated only if the local specific enthalpy is already determined, as will be shown in Sec. VII. Thus, the necessary data for ρ_∞ and ρ_w are not known. Therefore, to obtain a first overview of the local specific enthalpy distribution the theory of Pope [Eq. (3)] was used. With the values for the specific enthalpy, the species mass fractions can then be calculated (see Sec. VII). Finally, the extended theory of heat transfer [Eq. (4)] may be used to check the enthalpy values previously determined. These results are shown in Fig. 24.

The distributions obtained with Eq. (4) correspond very well to those obtained by Eq. (3). The maximum difference is about 5% at higher enthalpies, while with decreasing enthalpy the difference increases. The maximum enthalpies obtained with this method are 83.4 MJ/kg at x = 50 mm and 25.3 MJ/kg at x = 300 mm, respectively, at the center of the jet. Both values compare well with the maxima calculated with Eq. (3).

The integration of the distributions yields average specific enthalpies of 20.2 MJ/kg at x = 50 mm and 7.1 MJ/kg at x = 300 mm. Again, both values are similar to those calculated with Eq. (3) and with the value measured at the plasma source exit.

VII. Local Mass Flux

Very important and interesting parameters for the assessment of a plasma flow for the heat load simulation of TPS materials are the species mass fluxes. Furthermore, they are essential for any kind of computer simulation as inflow or boundary conditions and for validation of the different models used herein. While emission spectroscopic investigations, as they are used up to now, can only give qualitatively the composition of the plasma; in the following a method to approximate the different species concentrations is presented.

A. Basic Equations

If we assume the nitrogen plasma consisting of the species N_2, N, N^+, and e^-, their concentrations may be calculated from the energy equation if the specific enthalpy, heavy particle temperature, velocity, ambient pressure, and electron temperature are measured or known. The main assumptions are as follows.

1) The ambient pressure is equal to the static pressure in the flow.

2) Only single ionized atomic nitrogen is considered. This assumption is valid for high enthalpies and temperatures, where it may be assumed that nitrogen is nearly completely dissociated.

3) Quasineutrality—density of the ions is equal to the electron density.

4) A mixture of ideal gases with two temperatures $T_{rot} = T_{trans} = T_\infty$, $T_{vib} = T_e$.

The partial pressure of the electrons is given by

$$p_e = n_e k T_e \qquad (5)$$

The heavy particle density is therefore

$$n_h = [(p_\infty - p_e)/kT_\infty] \qquad (6)$$

The mole fractions of the electrons and the ions are

$$\Psi_e = \Psi_{N^+} = [n_e/(n_h + n_e)] \qquad (7)$$

The total mass conservation equation yields

$$\Psi_{N_2} + \Psi_N + 2\Psi_{N^+} = 1 \tag{8}$$

The energy conservation equation may be written

$$h_{t,\infty} = \tfrac{1}{2}v_\infty^2 + c_{p,\text{rot}+\text{trans}}T_\infty + \xi_{N_2}h_{\text{vib}} + \xi_N h_N + \xi_{N^+}h_{N^+} \tag{9}$$

where $c_{p,\text{rot}+\text{trans}}$ denotes the portion of the translational and rotational degrees of freedom (DOF) to the heat capacity at constant pressure, ξ_i are the species mass fractions, h_N is the dissociation enthalpy, h_{N^+} is the ionization enthalpy and h_{vib} the vibrational energy given in Ref. 24. For mixtures of ideal gases it follows:

$$c_{p,\text{rot}+\text{trans}} = \frac{f_M + 2}{2}\frac{\mathcal{R}}{M_M} \tag{10}$$

where $\mathcal{R}$ is the gas constant, f_M are the average translational ($f_{\text{trans}} = 3$) and rotational ($f_{\text{rot}} = 2$) DOF for the gas mixture, and M_M is the mole mass of the mixture:

$$\begin{aligned} f_M &= \Psi_N f_N + \Psi_{N_2} f_{N_2} + \Psi_{N^+} f_{N^+} + \Psi_e f_e \\ &= 5 - 2\Psi_N - 4\Psi_{N^+} \end{aligned} \tag{11}$$

$$M_M = \sum_i \Psi_i M_i = M_N(2 - 3\Psi_{N^+} - \Psi_N) \tag{12}$$

Therefore, the mass fractions are given by

$$\xi_i = \frac{M_i\Psi_i}{\sum_i \Psi_i M_i} \tag{13}$$

By substituting Eqs. (10–13) in Eq. (9), an equation for the atomic nitrogen mole fraction Ψ_N can be yielded.

B. Application to the Nitrogen Plasma Flow

With the calculated values for the local specific enthalpy (Sec. VI, theory of Pope[14–16]), measured ambient pressure and measured distributions for the velocity, electron density, temperature, and heavy particle temperature, it is now possible to calculate the local species mass and mole fractions of the pure nitrogen plasma flow. The results for the mole fractions at the inflow (x = 50 mm) and outflow (x = 300 mm) cross sections are shown in Figs. 25–28. Figures 29–32 depict the distributions of the species number densities. Multiplication of the species number densities with their velocity and mass yields local specific mass fluxes of the species. The sum of the species mass fluxes gives the total specific mass flow rate shown in Fig. 33.

The mole fraction of dissociated nitrogen is calculated to be about 60% and the fraction of the ions is nearly 20%. With increasing distance strong recombination occurs, leading to a dissociated mole fraction of about 68% and an ionized fraction

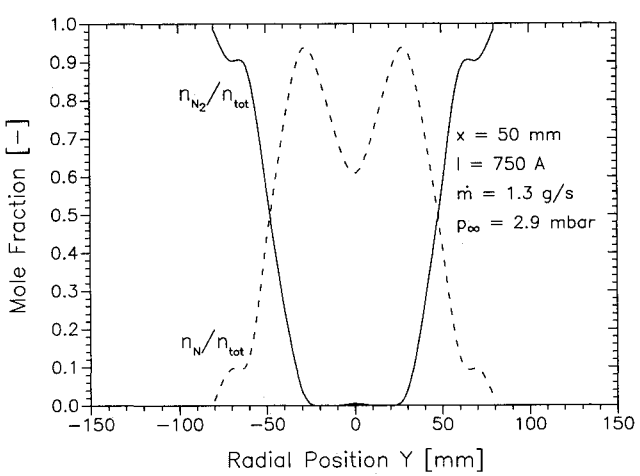

Fig. 25 Mole fraction distributions at a distance of x = 50 mm (species N and N_2).

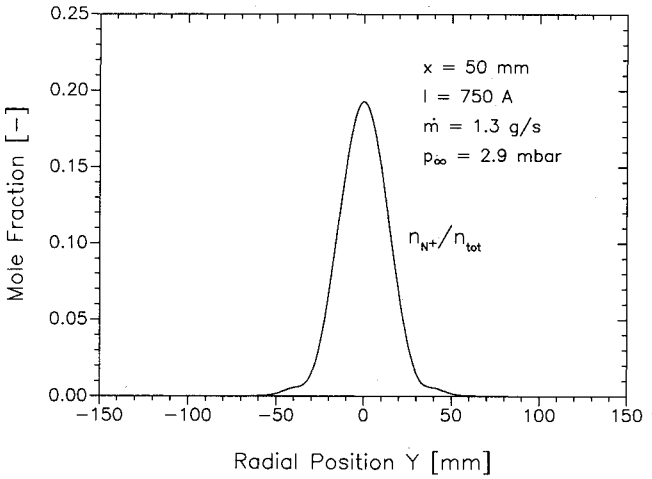

Fig. 26 Mole fraction distribution at a distance of x = 50 mm (species N^+).

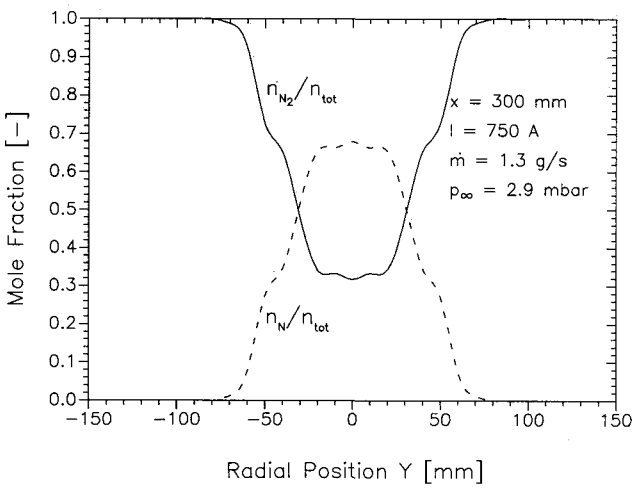

Fig. 27 Mole fraction distributions at a distance of x = 300 mm (species N and N_2).

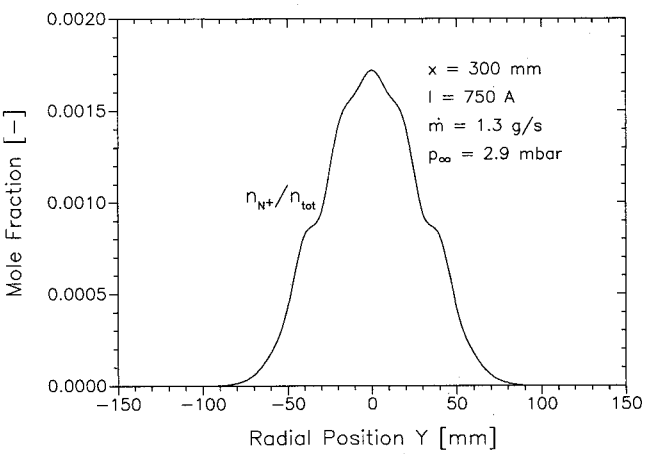

Fig. 28 Mole fraction distribution at a distance of x = 300 mm (species N^+).

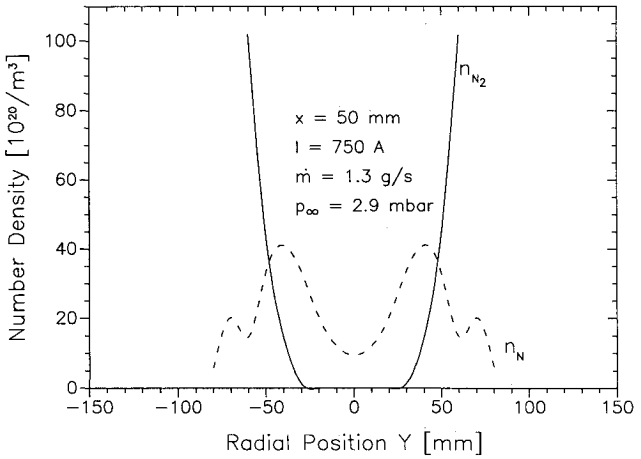

Fig. 29 Number density distributions at a distance of x = 50 mm (species N and N_2).

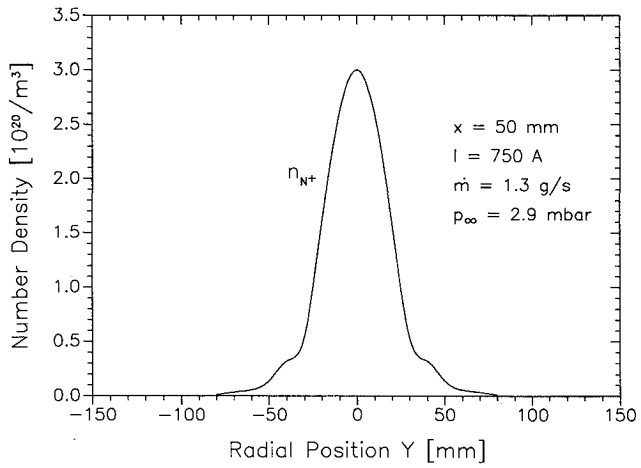

Fig. 30 Number density distribution at a distance of x = 50 mm (species N^+).

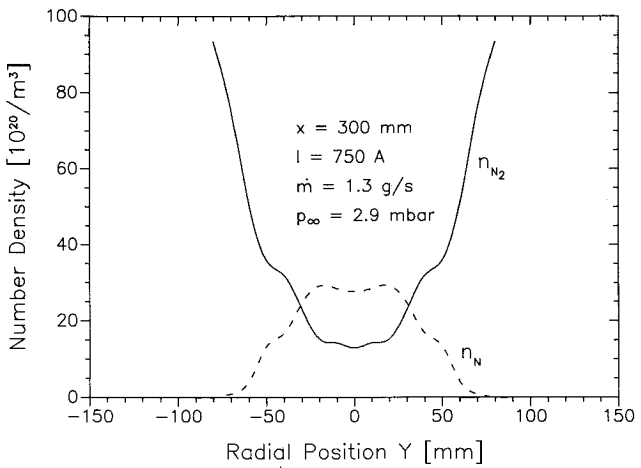

Fig. 31 Number density distributions at a distance of x = 300 mm (species N and N_2).

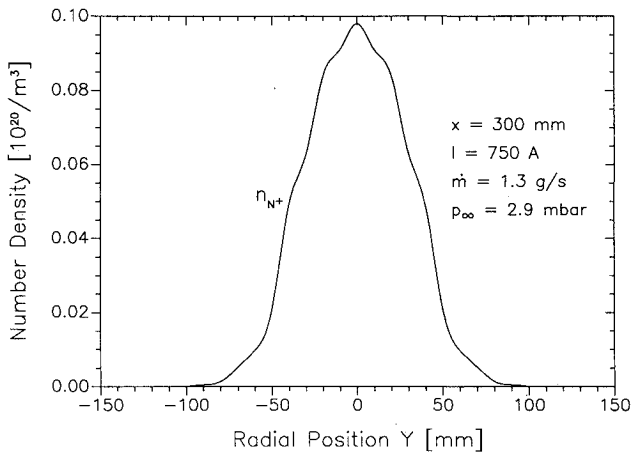

Fig. 32 Number density distribution at a distance of x = 300 mm (species N^+).

of only 0.17% at the position x = 300 mm. This is a very important result for the assessment of material tests, which are performed typically at such positions.

A very interesting value is the total specific mass flux at the center of the jet at the position x = 300 mm. This value is determined to be about 0.128 kg/(m²s) which is only 9.4% higher than the required value of 0.117 kg/(m²s) (see Sec. II). Thus, all required simulation values (local specific enthalpy, total pressure, and local specific mass flux) were reproduced within the PWK-IRS.

C. Verification of the Calculated Species Mass Fluxes

A verification of the obtained mole fractions is possible by integrating the total specific mass flux over the plasma jet diameter. This integration yields for the inflow cross section (x = 50 mm) a mass flow rate of $\dot{m}$ = 1.29 g/s, which compares very well to the mass flux fed through the plasma source (1.33 g/s). The calculated mass flux at the outflow cross section (x = 300 mm) is about 3.14 g/s, which is 2.36 times the input mass flux and which corresponds very well to the loss of the average specific enthalpy of the plasma flow due to the suction of ambient gas (about 2.4, see Sec. VI).

Additional verifications of the calculated values may be performed by applying the Bernoulli equation for compressible flows to calculate the total pressure and comparing it to the measured one. Basically Bernoulli's equation for compressible flows reads

$$(p_s/\rho_s) + u_s + \tfrac{1}{2}v_s^2 = (p_\infty/\rho_\infty) + u_\infty + \tfrac{1}{2}v_\infty^2 \qquad (14)$$

where u, p, ρ, and v denote the internal energy, pressure, density, and velocity, and the subscripts s and ∞ are for the stagnation point and freestream values, respectively. Therefore, the stagnation or total pressure is

$$p_{\text{tot}} = (\rho_s/\rho_\infty)p_\infty + \rho_s(u_\infty - u_s) + \tfrac{1}{2}\rho_s v_\infty^2 \qquad (15)$$

The ratio of the stagnation point temperature to the freestream temperature is

$$\frac{T_s}{T_\infty} = \left(1 + \frac{\kappa - 1}{2} Ma^2\right) \qquad (16)$$

Because of the relative low velocities and high temperatures in the freestream for the investigated test conditions, the temperature ratio reaches values of 1.0–1.05; the difference of the internal energies $u_\infty - u_s$ may therefore be neglected. Thus, the stagnation pressure is

$$p_{\text{tot}} = (\rho_s/\rho_\infty)p_\infty + \tfrac{1}{2}\rho_s v_\infty^2 \qquad (17)$$

The ratio of the stagnation point density to the freestream density is

$$(\rho_s/\rho_\infty) = (T_s/T_\infty)^{1/(\kappa-1)} \qquad (18)$$

with an effective ratio of the specific heats

$$\kappa \approx \frac{\bar{C}_p}{\bar{C}_v} = \frac{\bar{C}_p}{\bar{C}_p - \dfrac{\mathcal{R}}{M_M}} \qquad (19)$$

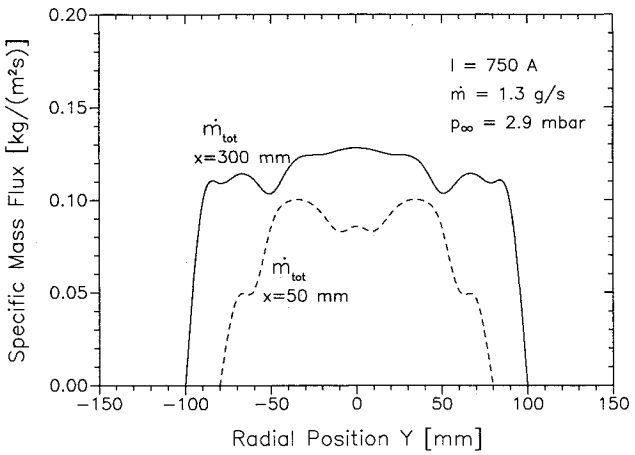

Fig. 33 Total specific mass flux distributions.

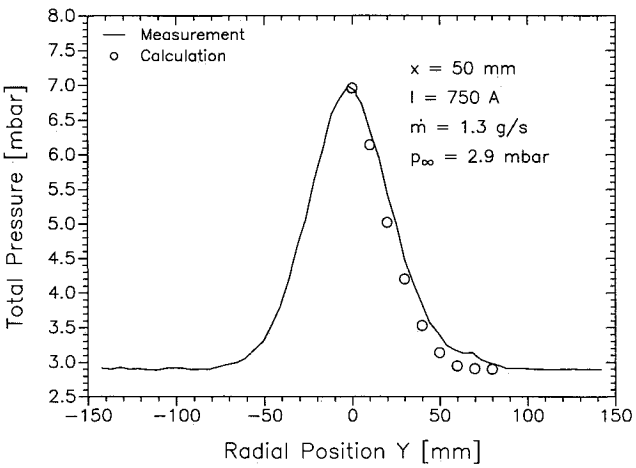

Fig. 34 Comparison of the calculated to the measured total pressure for x = 50 mm.

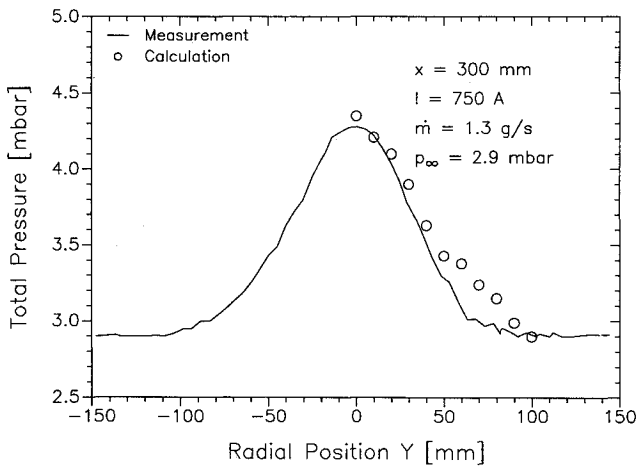

Fig. 35 Comparison of the calculated to the measured total pressure for x = 300 mm.

and a specific heat at constant pressure approximated by $\bar{C}_p \approx h_{t,\infty}/T_\infty$.

Comparisons of the calculated to the measured pressure for the two positions x = 50 mm and x = 300 mm are shown in Figs. 34 and 35. The agreement with the measured values is good (within 10%). Deviations may occur because of the high sensitivity of the presented method to small inaccuracies in the determination of the freestream velocity.

VIII. Summary and Conclusions

A nitrogen high-enthalpy plasma flow within a plasma wind tunnel was the subject of an experimental investigation at the Institut für Raumfahrtsysteme of the University of Stuttgart. Axial measurements (in flow direction) were performed to determine the stagnation pressure, heat flux, velocity, electron density, and temperature of the flowfield. Two cross sections were selected for measurements of radial distributions. With these measurements it was possible to calculate the local specific enthalpies, mass fluxes, and number densities of molecular, atomic, and ionized nitrogen.

The conditions at the second cross section were chosen to simulate the maximum heat load for a possible trajectory of HERMES. About 68% of the nitrogen is dissociated at the center of the plume, while the ionized mole fraction is only about 0.17%. The integration of the local mass flux distributions shows that the flow is sucking in and accelerating the ambient gas, and thus lowering the specific energy. The total mass flux of 3.14 g/s at this position is about 2.4 times the flux through the plasma source, and, corresponding to this, the mean specific enthalpy is only about 40% of the value at the plasma source exit. The heat flux on a cooled copper surface at the center of the jet is here 530 kW/m^2, the total pressure 4.3 mbar, the total local mass flux reaches 0.128 kg/(m^{2}s), and the specific enthalpy is 26.6 MJ/kg. All these conditions are in good agreement (within 10%) with the required conditions of a possible trajectory of HERMES.

At the first cross section (distance 50 mm to the plasma source) and at the center of the jet, the flow is up to 60% dissociated and 20% ionized. The maximum specific enthalpy reaches 86.6 MJ/kg, the total pressure is 7 mbar, and the heat flux is about 2300 kW/m^2. The average specific enthalpy at this position was calculated to be about 20–21 MJ/kg (21.5 MJ/kg with the theory of Pope[14–16] and 20.2 MJ/kg with Fay and Riddell[22]), which corresponds well with the average enthalpy measured in the plasma source (19.3 MJ/kg). The integration of the total local mass flux distribution yields a mass flow rate of 1.29 g/s, which again corresponds well with the mass flux fed through the plasma source.

The determination of the species number densities, the temperatures, and velocities now gives the possibility to validate the numerical methods used for the calculation of nonequilibrium flows.

Further investigation of these test conditions is planned with nonintrusive measurement techniques, i.e., emission spectroscopy and Fabry-Perot interferometry. It is also planned to use probes of different catalytic behavior to approximate the degree of dissociation of the flow and verify the method presented in this article. Additionally, the numerical calculation of the plasma source to obtain and compare the local mass fluxes at the first cross section is in preparation.

The extension to an air plasma flow will then be the next iteration step of this research program.

Acknowledgments

The authors wish to thank all co-workers of the PWK-simulation group at the IRS for their assistance in performing the experiments. This work was supported by the Aviation Marcel Dassault under Grant H-ST-1-1135-AMD.

References

[1]Auweter-Kurtz, M., Laure, S., Messerschmid, E., Röck, W., and Tubanos, N., "The IRS Plasma Wind Tunnels for the Investigation of Thermal Protection Materials for Reentry Vehicles," *Proceedings of the First European Symposium on Aerothermodynamics for Space Vehicles*, European Space Research and Technology Centre, Noordwijk, The Netherlands, May 1991, pp. 283–293.

[2]Auweter-Kurtz, M., Eppler, J., Kurtz, H., Loesener, O., Messerschmid, E., and Mulzer, E., "Arc Heated High Enthalpy Channel for Thermal Protection Systems of Spacecrafts," *Proceedings of the 4th European Symposium on Spacecraft Materials in Space Environ-*

ment, Centre d'Etudes et de Recherches de Toulouse, Toulouse, France, Sept. 1988, pp. 75–84.

[3]Schönemann, A., et al., "The Plasma Wind Tunnels PWK1 and PWK2," Inst. für Raumfahrtsysteme, Univ. Stuttgart, Internal Rept. IRS 92-P6, Stuttgart, Germany, July 1992.

[4]Auweter-Kurtz, M., "Lichtbogenantriebe für Weltraumaufgaben," B. G. Teubner, Stuttgart, Germany 1992.

[5]Loesener, O., Auweter-Kurtz, M., Hartling, M., and Messerschmid, E. W., "Linear Pyrometer for Investigations of Thermal Protection Systems," *Journal of Thermophysics and Heat Transfer*, Vol. 7, No. 1, 1993, pp. 82–87.

[6]Fasoulas, S., Auweter-Kurtz, M., Früholz, H., Gogel, T. H., Habiger, H., Hilfer, G., Laure, S., and Sleziona, P. C., "Experimental and Computational Investigation of the High Enthalpy Flow Within the Plasma Wind Tunnel PWK-IRS," Inst. für Raumfahrtsysteme, Univ. Stuttgart, Interim Repts. IRS-92-P3 and IRS-92-P8, Stuttgart, Germany, 1992.

[7]Fasoulas, S., Auweter-Kurtz, M., Früholz, H., Gogel, T. H., Habiger, H., Hilfer, G., Laure, S., and Sleziona, P. C., "Experimental and Computational Investigation of the High Enthalpy Flow Within the Plasma Wind Tunnel PWK-IRS," Inst. für Raumfahrtsysteme, Univ. Stuttgart, Final Rept. IRS-92-P13, Stuttgart, Germany, 1992.

[8]Elsner, M., "Thermal Protection System Comparison of the HERMES Flight Environment and Test Facility Environment of the IRS Plasma Wind Tunnel," Messerschmidt-Bölkow Blohm Rept. H-NT-1B-0006-MBB, Oct. 1990.

[9]Koppenwallner, G., "Kraft- und Wärmeübergangsmessung in Hyperschallströmungen Geringer Gasdichte," 9. Lehrgang für Raumfahrttechnik, Göttingen, Germany, March 1971.

[10]Swift, J. W., and Schawr, M. J. R., "Electric Probes for Plasma Diagnostics," Ilille Book Ltd., London, 1970.

[11]Chen, F., "Electric Probes," *Plasma Diagnostic Techniques*, Academic Press, London, 1965, pp. 113–200.

[12]Chen, S. L., and Sekiguchi, T., "Instantaneous Direct Display System of Plasma Parameters by Means of Triple Probe," *Journal of Applied Physics*, Vol. 36, No. 8, 1965, pp. 2363–2375.

[13]Bohn, W. L., Beth, M.-U., and Nedder, G., "On Spectroscopic Measurements of Velocity Profiles and Nonequilibrium Radial Temperatures in an Argon Plasma Jet," *Journal of Quantitative Spectroscopy & Radiative Transfer*, Vol. 7, Pergamon, London, 1967, pp. 661–676.

[14]Vojvodich, N. S., and Pope, R. B., "The Influence of Ablation on Stagnation Region Convective Heating for Dissociated and Partially Ionized Boundary Layer Flows," *Proceedings of the 1965 Heat Transfer and Fluid Mechanics Institute*, Stanford Univ. Press, Stanford, CA, June 1965, pp. 114–137.

[15]Marvin, J. G., and Pope, R. B., "Laminar Convective Heating and Ablation in the Mars Atmosphere," *AIAA Journal*, Vol. 5, No. 2, 1967, pp. 240–248.

[16]Pope, R. B., "Measurements of Enthalpy in Low Density Arc Heated Flows," *AIAA Journal*, Vol. 6, No. 1, 1968, pp. 103–110.

[17]Pope, R. B., "Stagnation Point Convective Heat Transfer in Frozen Boundary Layers," *AIAA Journal*, Vol. 6, No. 4, 1968, pp. 619–626.

[18]Boison, J. C., and Curtiss, H. A., "An Experimental Investigation of Blunt Body Stagnation Point Velocity Gradient," *ARS Journal*, Vol. 29, No. 2, 1959, pp. 130–135.

[19]Goulard, R., "On Catalytic Recombination Rates in Hypersonic Stagnation Heat Transfer," *Jet Propulsion*, Vol. 28, No. 11, 1958, pp. 733–745.

[20]Park, C., "Nonequilibrium Air Radiation (NEQAIR) Program: User's Manual," NASA-TM-86707, July 1985.

[21]Gogel, T. H., and Messerschmid, E. W., "Radiation Transport Database," Inst. für Raumfahrtsysteme, Univ. Stuttgart, Study Note 3.1.2, Stuttgart, Germany, 1992.

[22]Fay, J. A., and Riddell, F. R., "Theory of Stagnation Point Heat Transfer in Dissociated Air," *Journal of the Aeronautical Sciences*, Vol. 25, No. 2, 1958, pp. 73–85.

[23]Rosner, D. E., "Similitude Treatment of Hypersonic Stagnation Point Heat Transfer," *ARS Journal*, Vol. 29, No. 3, 1959, pp. 215, 216.

[24]Vincenti, W. G., and Kruger, C. H., "Introduction to Physical Gas Dynamics," Wiley, New York, 1965.